SCIENCE CHINA
Chemistry

•ARTICLES•

October 2018 Vol.61 No.10: 1328–1337
https://doi.org/10.1007/s11426-018-9260-2

Fluorination vs. chlorination: a case study on high performance organic photovoltaic materials

Yun Zhang[1,2], Huifeng Yao[1*], Shaoqing Zhang[1,3], Yunpeng Qin[1,3], Jianqi Zhang[4], Liyan Yang[1,2], Wanning Li[1,2], Zhixiang Wei[4], Feng Gao[5] & Jianhui Hou[1,2*]

[1]*State Key Laboratory of Polymer Physics and Chemistry, Beijing National Laboratory for Molecular Sciences, CAS Research/Education Center for Excellence in Molecular Sciences, Institute of Chemistry, Chinese Academy of Sciences, Beijing 100190, China;*
[2]*University of Chinese Academy of Sciences, Beijing 100049, China;*
[3]*School of Chemistry and Biological Engineering, University of Science and Technology Beijing, Beijing 100083, China;*
[4]*Key Laboratory of Nanosystem and Hierarchical Fabrication, National Center for Nanoscience and Technology, Beijing 100190, China;*
[5]*Department of Physics, Chemistry and Biology (IFM), Linköping University, Linköping SE-581 83, Sweden*

Received March 30, 2018; accepted April 16, 2018; published online June 20, 2018

Halogenation is a very efficient chemical modification method to tune the molecular energy levels, absorption spectra and molecular packing of organic semiconductors. Recently, in the field of organic solar cells (OSCs), both fluorine- and chlorine-substituted photovoltaic materials, including donors and acceptors, demonstrated their great potentials in achieving high power conversion efficiencies (PCEs), raising a question that how to make a decision between fluorination and chlorination when designing materials. Herein, we systemically studied the impact of fluorination and chlorination on the properties of resulting donors (PBDB-T-2F and PBDB-T-2Cl) and acceptors (IT-4F and IT-4Cl). The results suggest that all the OSCs based on different donor and acceptor combinations can deliver good PCEs around 13%–14%. Chlorination is more effective than fluorination in downshifting the molecular energy levels and broadening the absorption spectra. The influence of chlorination and fluorination on the crystallinity of the resulting materials is dependent on their introduction positions. As chlorination has the advantage of easy synthesis, it is more attractive in designing low-cost photovoltaic materials and therefore may have more potential in large-scale applications.

organic solar cells, bandgap engineering, fluorination, chlorination

Citation: Zhang Y, Yao H, Zhang S, Qin Y, Zhang J, Yang L, Li W, Wei Z, Gao F, Hou J. Fluorination vs. chlorination: a case study on high performance organic photovoltaic materials. *Sci China Chem*, 2018, 61: 1328–1337, https://doi.org/10.1007/s11426-018-9260-2

1 Introduction

Bulk heterojunction organic solar cells (OSCs) based on an electron donor and an electron acceptor provide an efficient way to convert sunlight photons to electricity, which attract much attention all around the world due to their advantages of low-cost, flexibility and lightweight [1–4]. The development and application of highly efficient photovoltaic materials including donor and acceptor contribute greatly to the rapidly increasing of the power conversion efficiencies (PCEs) [5–19]. In early reports, homopolymers like P3HT and fullerene derivatives like [6,6]-phenyl-C61/C71-butyric acid methyl ester (PCBM) were the most widely used donors and acceptors, respectively. Since these donor:acceptor combinations have poor absorption spectra and difficultly tunable molecular energy levels, the resulting OSCs usually had relatively low short-circuit current (J_{SC}) and open-circuit voltage (V_{OC}), and the top PCEs were limited at ~4%–5% [20–22]. Since about 2006, the donor-acceptor structures have been introduced to modulate the intramolecular charge

*Corresponding authors (email: yaohf@iccas.ac.cn; hjhzlz@iccas.ac.cn)

© Science China Press and Springer-Verlag GmbH Germany, part of Springer Nature 2018

transfer of polymer donors, leading to the great tunability of absorption spectrum and molecular energy levels [23,24]. Recently, the acceptor-donor-acceptor (A-D-A)-type small molecules are emerging as very promising non-fullerene electron acceptors, replacing the leading role of fullerene derivatives in OSCs gradually [17,25–28]. The OSCs based on these materials maximize the V_{OC} and J_{SC} values and thus obtained PCE of over 13% [29–33].

The performances of the photovoltaic materials are closely associated with the properties such as orbital energy levels, density distribution and mobility [34]. Over the past decade, researchers have developed many molecular design strategies to modulate the π electron behaviors in the intra- and inter-molecules. For example, introducing functional groups with electron withdrawing properties like ester and carbonyl can effectively down-shift the highest occupied molecular orbital (HOMO) and lowest unoccupied molecular orbital (LUMO) levels [35,36]; incorporation of electron donating groups like alkoxy can obviously broad the absorption spectrum [37,38]. Halogenation has been proved as one of the most efficient chemical modification strategies and yielded many excellent donors and acceptors [39–44]. As fluorine is the most electronegative atom with a very small size, fluorination can effectively modulate the π electron properties and meanwhile avoid causing large steric hindrance for molecular packing [45]. Furthermore, the fluorine-containing materials always have enhanced crystallinity resulted from noncovalent intermolecular interactions of F···H, F···S, and so on [46]. These advantages contribute to the design of many excellent donors (polymers like PTB7-Th [47], PBDT-TS1 [48], PffBT4T-2OD [49,50], PBDB-T-2F [30,33], FTAZ [51]; small molecules like BTID-2F [52]) and acceptors (such as IT-4F [29], INIC3 [53], IEICO-4F [54], IUIC [55] and NITI [56]).

Chlorination is also a very common method used in modifying the π electron behaviors of organic semiconductors and achieved many good results [43]. Even though chlorine (electronegativity, 3.16) is less electronegative than fluorine (electronegativity, 3.98), its empty 3D orbit may help to accept the π electrons in the system, leading to the stronger ability of chlorination than fluorination in downshifting the molecular energy levels. The higher dipole moment of chlorine-carbon bond than that of fluorine-carbon bond can enhance the intramolecular charge transfer effect and thus broaden the absorption spectrum [57,58]. As chlorine has a bigger size than fluorine, the influence of chlorination on the intermolecular packing of the resulting materials should be taken into consideration carefully. Furthermore, in comparison with fluorine-containing materials, the chlorine-containing materials is more easily to synthesize, therefore, the material cost is relatively low. In 2016, He *et al.* [59] synthesized the chlorinated benzothiadiazole unit and used it to construct the polymer donor, which achieved good photovoltaic performance. In our group, we designed the chlorinated polymer donor (PBDB-T-2Cl [60]) and acceptors (IT-4Cl [58] and IEICO-4Cl [57]). These chlorinated donors or acceptors yielded PCEs in single-junction and tandem OSCs, suggesting their great potentials in further applications.

These recent results raise a question that how to make a choice between fluorination and chlorination when designing highly efficient photovoltaic materials. To provide a direct comparison, herein, we selected two polymer donors and two non-fullerene small molecules acceptors including the fluorine-containing donor PBDB-T-2F, the chlorine-containing donor PBDB-T-2Cl, the fluorine-containing acceptor IT-4F and chlorine-containing acceptor IT-4Cl (Figure 1(a)), to study the difference of halogenation on the properties of donors and acceptors. The molecular weight of polymer donors is summarized in Table S1 (Supporting Information online). We found that chlorination could downshift both the HOMO and LUMO levels greater than fluorination. The absorption edges between PBDB-T-2F and PBDB-T-2Cl do not show much difference while that of IT-4Cl is obviously red-shifted than IT-4F. The replacement of fluorine atoms with chlorine atoms decreases the crystallinity on the polymer donor while it increased the crystallinity of the small molecule acceptors. All the four OSCs based on the different donor:acceptor combinations show representative PCEs around 13%–14%. These results suggest that if chlorination does not cause bad effects on the molecular packing, it would be a good candidate for designing highly efficient resulting materials due to its easy synthetic procedures.

From the synthesis of point view, introduction of chlorine atoms on organic semiconductors is much easier than introduction of fluorine atoms. As displayed in Figure 1(b), 3-chloro-2-alkylthiophene and 3-fluoro-2-alkylthiophene are two very important intermediates for obtaining the polymer PBDB-T-2Cl and PBDB-T-2F, respectively. The synthesis of chlorine-containing compound is just one-step procedure at high yield while the synthesis of its fluorine-containing counterpart takes four steps. Similar phenomenon is existed in the preparations of small molecule acceptors of IT-4F and IT-4Cl. The reason is that the fluorine-containing materials are usually synthesized from other halogen-containing precursors via exchange reactions [61–64]. For example, the bromine-fluorine exchange reaction produces the 3-fluoro-2-alkylthiophene, and the chlorine-fluorine exchange reaction yields the terminal group of IT-4F. These reactions are usually taken at rigorous conditions at relatively low yields. For example, step 3 for the target 3-fluoro-2-alkylthiophene occurs at very low temperature about –100 °C, and step 1 for the end-ground of IT-4F reacts at temperature as high as ca. 200 °C. These features result in a fact that the fluorine-containing materials are much expensive than their chlorine-containing counterparts. As the PCEs of the OSCs are

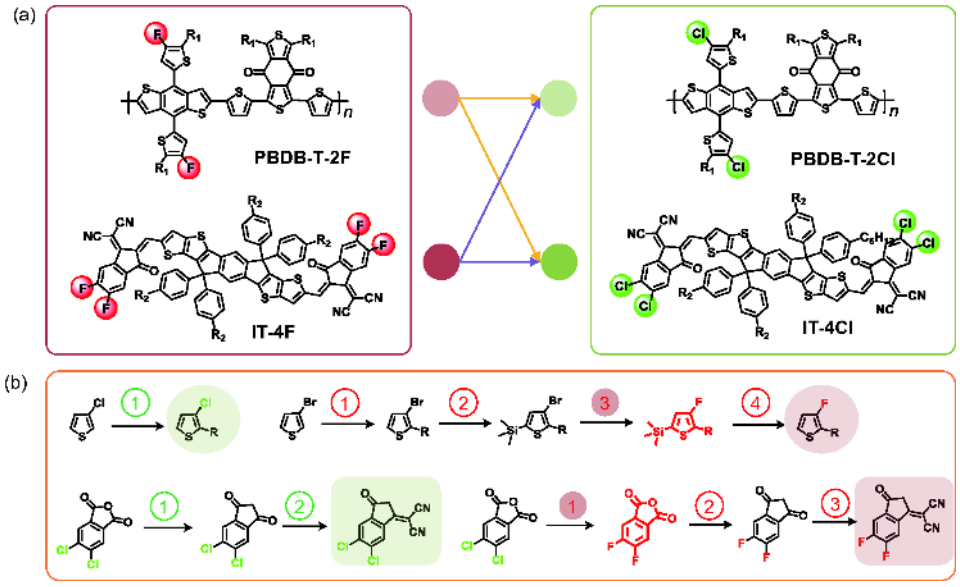

Figure 1 (a) Molecular structures of the fluorinated polymer donor and small molecule acceptor (left) and chlorinated polymer donor and small molecule acceptor (right). (b) The synthetic procedures of fluorinated and chlorinated intermediates (color online).

reaching the threshold for practical applications, the material cost should be as low as possible for large-scale production; therefore, chlorination has more advantages than fluorination at this point.

2 Experimental

2.1 Materials

PBDB-T-2F and PFN-Br were purchased from Solarmer Materials Inc. (China). PEDOT:PSS, Clevios™ P VP AI4083, was commercially available from Heraeus (Germany). The other solvents were commercially available and used as received.

2.2 Device fabrication

The mixed solutions of polymer:IT-4F were dissolved in chlorobenzene at a polymer concentration of 10 mg/mL (polymer/solvent), and then stirred at least 6 h at 40 °C. The blends of polymer:IT-4Cl were dissolved in chloroform at a polymer concentration of 7 mg/mL, and then stirred more than 6 h at room temperature. The ratio of donor versus acceptor was fixed at 1:1. The PFN-Br solution was prepared in methanol at a concentration of 0.5 mg/mL and then stirred more than 6 h at room temperature. The indium tin oxide (ITO) glasses were pre-cleaned by surfactant, deionized water, acetone and isopropanol in an ultrasonic bath. Then UV-ozone treatment was optimized ITO surface for 15 min. The PEDOT:PSS film made by spin-coating (~30 nm thickness), following annealing treatment at 150 °C for 15 min. After transfer ITO substrate with PEDOT:PSS film into the glove box of nitrogen atmosphere, the blend solution was spin-coating on the PEDOT:PSS layer. The thicknesses of active layers are about 100 nm. Subsequently, the active layer was baked on hot plate at 100 °C for 10 min. The PFN-Br solution was spin-coating onto active layer after the substrate cooling to room temperature. Finally, 100 nm Al was deposited under high vacuum (~3×10^{-4} Pa) as cathode.

2.3 Instruments and measurements

The UV-visible absorption spectroscopy measurements of solutions and films were conducted on a Hitachi UH4150 spectrophotometer (Japan). The mobilities of hole and electron were obtained with Space Charge Limited Current (SCLC) method. The device architectures of hole-only and electron-only are ITO/PEDOT:PSS/active layer/Au and ITO/ZnO/active layer/Al, respectively. The mobility was calculated with the Mott-Gurney equation in the SCLC region.

$$J = \frac{9\varepsilon_0\varepsilon_r\mu V^2}{8d^3}, \quad (1)$$

which J is the space charge limited current, ε_0 is the permittivity of free space, ε_r is the relative permittivity of the material, d is the film thickness of active layer, V is the effective voltage.

The photo-CELIV and TPV measurements were performed by the all-in-one characterization platform Paios developed and commercialized by Fluxim AG (Switzerland). The carrier mobilities (μ) were calculated follow Eq. (2),

$$\mu = \frac{2d^2}{3At_{max}^2[1+0.36\frac{\Delta j}{j(0)}]}, \text{ if } \Delta j \le j(0). \quad (2)$$

where d is the active layer thickness, A is the voltage rise

speed, t_{max} is the time corresponding to the extraction peak maximum, and $j(0)$ is the displacement current.

The 2-D GIWAXS data were obtained on a XEUSS SAXS/WAXS SYSTEM (XENOCS, France) at the National Center for Nanosicence and Technology (NCNST, China). The tapping mode Atom Force Microscopy (AFM) measurements were acquired on a Nanoscope V (Vecco, USA) AFM. The transmission electron microscopy (TEM) photo images were performed on a Tecnai G2 F20 U-TWIN TEM instrument. The film thickness was measured by the Bruker Dektak XT profilometer (Germany). The *J-V* measurements were performed via the solar simulator (SS-F5-3A, Enlitech) along with AM 1.5G spectra, which was calibrated by the certified standard silicon solar cell (SRC-2020, Enlitech) at 100 mW/cm^2. The external quantum efficiency (EQE) data were obtained by using the solar-cell spectral-response measurement system (QE-R, Enlitech).

3 Results and discussion

3.1 Theoretical analyses of fluorination and chlorination

In order to study the influences of halogen atoms on the molecular configurations and the orbital distributions, we performed theoretical calculation on the single-molecule models by using density functional (DFT) B3LYP with the 6-31G (d, p) basis set [65]. As shown in Figure S1 (Supporting Information online), there is no obvious change on the molecular configurations between the two polymers or the two acceptors. The dihedral angles between halogen-containing thiophene and BDT units in the PBDB-T-2Cl is slightly larger than that in PBDB-T-2F, which may be related to the larger size of chlorine than fluorine. The HOMO and LUMO distributions on the donors or the acceptors are not affected by the different halogenations. As shown in Figure 2(a), we then plot the total density of states (DOS) for the four molecule models at a range of –10–0 eV. The main differences of the DOS distributions between the fluorinated and chlorinated materials locate at both ends (high-energy region over –2 eV, low-energy region below –7 eV) while the intermediate region covering the HOMO and LUMO shows very close DOS distributions. In comparison with the fluorinated donor and acceptor, their chlorinated counterparts possess lower HOMO and LUMO levels. For the donors of PBDB-T-2F and PBDB-T-2Cl, the calculated bandgaps are identical. Differently, chlorinated acceptor IT-4Cl shows decreased bandgap than the fluorinated acceptor IT-4F by 20 meV. These results imply that chlorination is more effective than fluorination in down-shifting the energy levels and the bandgap can be narrowed in the chlorinated systems than that of fluorinated materials.

As shown in Figure 2(b), we also calculated the absorption spectra of the four molecular models via time-dependent DFT theory with B3LYP/6-31G (d, p) basis set, where ten excited states were performed. The two polymer donors show almost overlapped absorption spectra. PBDB-T-2Cl shows slightly higher molar absorption coefficient than PBDB-T-2F. For the two acceptors, when compared with IT-4F, the main absorption peak of IT-4Cl is red-shifted by 13 nm, and the molar absorption coefficient of IT-4Cl is much higher. These results suggest that chlorine-containing materials have better absorption properties than their fluorine-containing counterparts at a molecule level.

3.2 Optical properties, energy alignment and mobility characteristics

The UV-Vis absorption spectra of the donors and acceptors in thin films are shown in Figure 3(a). For the polymer donors, PBDB-T-2F show about 5 nm red-shift of the main peak when compared to PBDB-T-2Cl (8.66×10^4 cm^{-1}), and maximum extinction coefficient of PBDB-T-2F (9.10×10^4 cm^{-1}) is slightly higher than that of PBDB-T-2Cl. These results are not consistent with the theoretical calculations on molecular models. We think this is associated with stronger

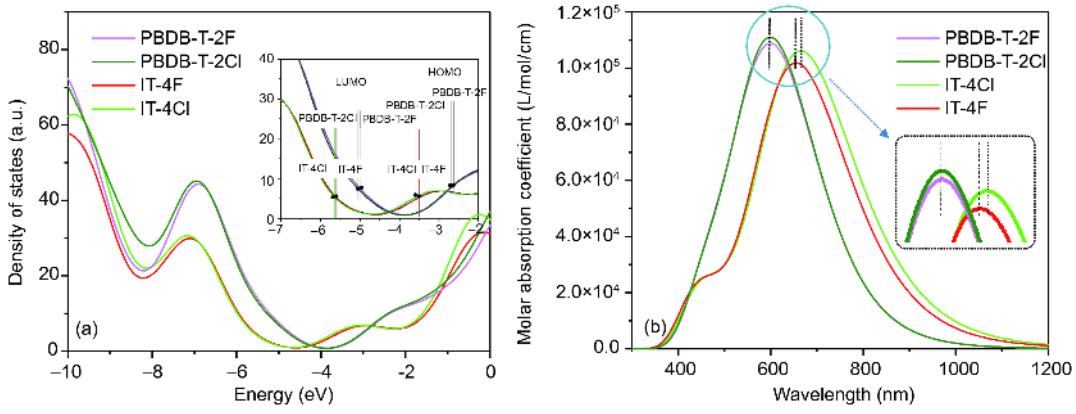

Figure 2 (a) DOS distributions and (b) calculated ultraviolet visible (UV-Vis) absorption of the four materials (color online).

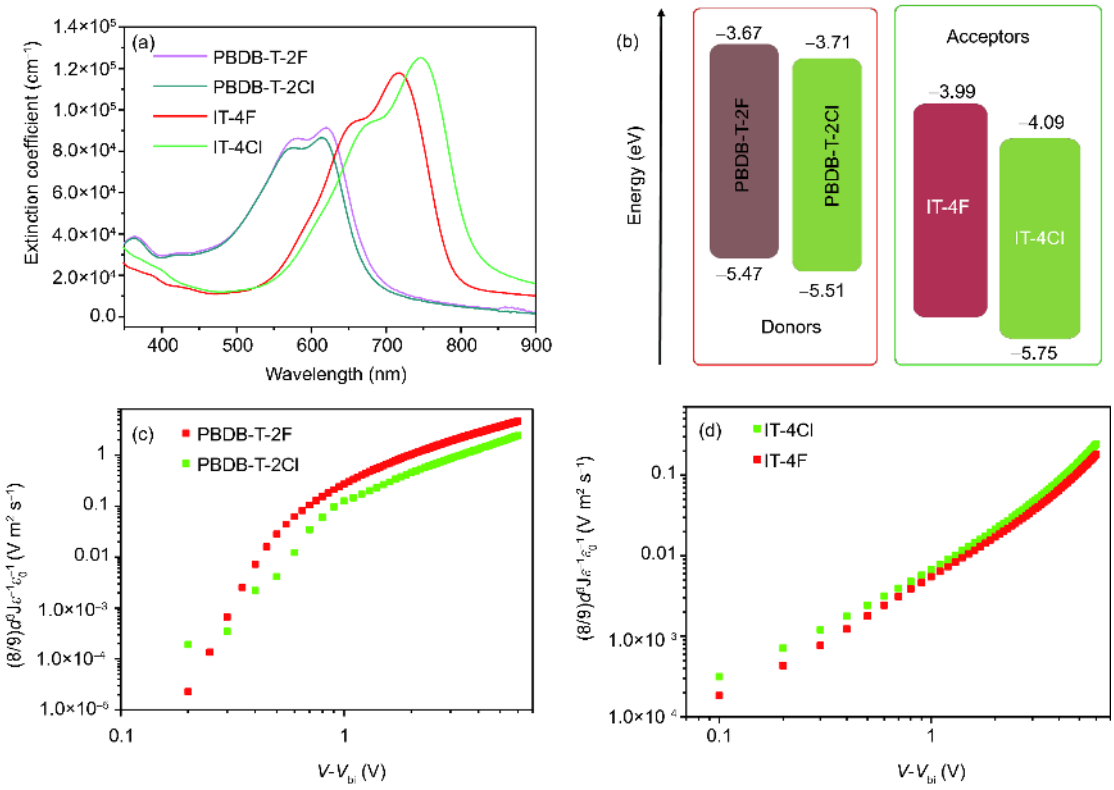

Figure 3 (a) Absorption spectra and (b) energy level alignment diagram of the four materials. SCLC date for (c) hole-only devices fabricated by neat polymer donors and (d) electron-only devices fabricated by neat small molecule acceptors (color online).

aggregation of molecules in the PBDB-T-2F film than that in PBDB-T-2Cl film, and we will investigate their difference of crystallinity later. The absorption onsets of the two polymer donors are very close, implying that they have the same optical bandgap (E_g^{opt}). For the two acceptors, IT-4Cl film displays a clear red-shifted absorption main peak than IT-4F by 30 nm, and the maximum extinction coefficient of IT-4Cl (1.26×10^4 cm^{-1}) is much higher than IT-4F (1.18×10^4 cm^{-1}). From these results, we can find that the influence of halogenation on the absorption spectra of the resulting materials is not only determined by molecules, but also related to the aggregation structures.

We measured the ionization potentials (IPs) and electron affinities (EAs) of the four materials in parallel via electrochemical cyclic voltammetry and plotted the energy level alignment diagram as Figure 3(b). As the EAs of the donor are very hard to measure, we estimated them by using their E_g^{opt}s (EA=IP+E_g^{opt}). We can find that both the IPs and EAs of chlorinated donor and acceptor are lower their fluorinated counterparts. The IPs of PBDB-T-2Cl and IT-4Cl are about 50 meV lower than that of PBDB-T-2F and IT-4F, respectively. It is should be noted that the IT-4Cl (–5.09 eV) has an EA about 100 meV lower IT-4F (–4.99 eV), resulting a narrowed electrochemical bandgap, which is consistent with the calculation results. We investigated the charge transport properties of the neat films via SCLC method. Hole-only devices with a structure of ITO/PEDOT:PSS/polymer/Au, electron-only devices with a structure of ITO/ZnO/acceptor/Al, were used to measure the hole and electron mobilities of the donors and acceptors, respectively. From the curves in Figure 3(c, d), the hole mobilities of PBDB-T-2F and PBDB-T-2Cl are calculated to be 2.44×10^{-4} and 1.05×10^{-4} cm^2 V^{-1}s^{-1}, and the electron mobilities of IT-4F and IT-4Cl are estimated to be 3.25×10^{-4} and 3.97×10^{-4} cm^2 V^{-1} s^{-1}. For the polymer donors, the fluorinated material has higher hole transport property than the chlorinated material. By contrary, for the small molecule acceptors, the chlorinated material possesses superior electron transport property than the fluorinated one.

3.3 Properties of molecular aggregation

In order to investigate the influences of fluorination and chlorination on the molecular aggregation behaviors for the donors and acceptors, we examined the crystalline properties of the four materials by grazing-incidence wide-angle X-ray scattering (GIWAXS). As displayed in Figure 4, both the PBDB-T-2Cl and PBDB-T-2F films show a face-on orientation with respect to the substrates. In the out-of-plane (OOP) direction, the (010) diffraction peaks of the two

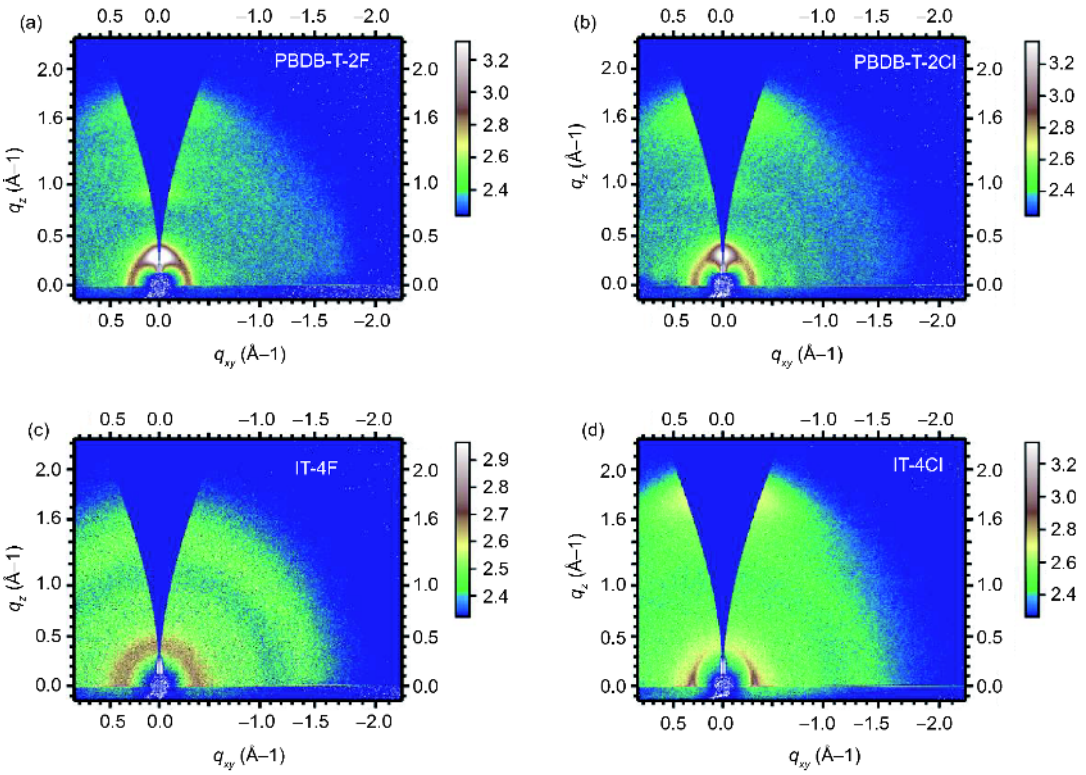

Figure 4 2D GIWAXS patterns of the neat (a) PBDB-T-2F, (b) PBDB-T-2Cl, (c) IT-4F and (d) IT-4Cl films (color online).

polymer films locate at almost the same position of q_z= 1.65 Å^{-1} (see q_z line cuts of the corresponding GIWAXS patterns in Figure S2), corresponding of a π-π interaction distance of 3.81 Å. The OOP lamellar (h00) peaks of PBDB-T-2F are stronger than that of PBDB-T-2Cl, suggesting PBDB-T-2F has more ordered packing than PBDB-T-2Cl. This may be resulted from the larger size of chorine atom than fluorine atom and contribute to the enhanced extinction coefficient of PBDB-T-2F film than that of PBDB-T-2Cl film. For the two acceptors, the OOP (010) of IT-4F is a diffuse ring locates at q_z around 1.78 Å^{-1} while IT-4Cl has a pronounced peak locates at q_z=1.65 Å^{-1}. The corresponding π-π stacking distances of IT-4Cl and IT-4F are 3.53 and 3.81 Å, suggesting that IT-4Cl shows more ordered packing with a strong face-on orientation. From these results, we can conclude that the influence of fluorination and chlorination on the crystalline properties of the resulting materials is highly dependent on the positions of halogen atoms on the systems.

3.4 Photovoltaic properties and morphological characteristics

3.4.1 Photovoltaic properties

To further investigate the differences between fluorination and chlorination on the photovoltaic performance of the resulting materials, we fabricated four OSCs based on different donor:acceptor combinations, including PBDB-T-2F:IT-4F, PBDB-T-2F:IT-4Cl, PBDB-T-2Cl:IT-4F and PBDB-T-2Cl:IT-4Cl. We adopt the same structure of ITO/PEDOT:PSS/donor:acceptor/PFN-Br/Al to fabricate the OSCs, and the processing conditions were kept the same as well. The normalized absorption spectra of the blend films are shown in Figure 5(a), from which we can find that IT-4Cl-based films have obvious red-shifted absorption spectra than IT-4F-based films and the absorption intensity of IT-4Cl-based films are much higher than IT-4F-based films. These features should be ascribed to the strong absorption of IT-4Cl than that of IT-4F in the long wavelength region and will contribute to higher J_{SC} in the resulting IT-4Cl-based OSCs. Figure 5(b) depicts the photoluminescence (PL) spectra of the neat and blend films. The PL emission of the polymers can be quenched sufficiently in the four blends, suggesting the photoinduced charge transfer in the varied donor:acceptor blends is very efficient.

The current density-voltage (*J-V*) curves are shown in Figure 5(c) and the detailed photovoltaic parameters are collected in Table 1. Impressively, all the OSCs can obtain very good PCEs in a range from 12.67% to 14.29%. The OSCs based on IT-4Cl-containing donor:acceptor combinations including PBDB-T-2F:IT-4Cl and PBDB-T-2Cl:IT-4Cl have much higher J_{SC} around 22 mA cm^{-2}, while the OSCs based on IT-4F-contaning donor:acceptor combinations show a litter lower J_{SC} of ca. 21 mA cm^{-2}. The differences of

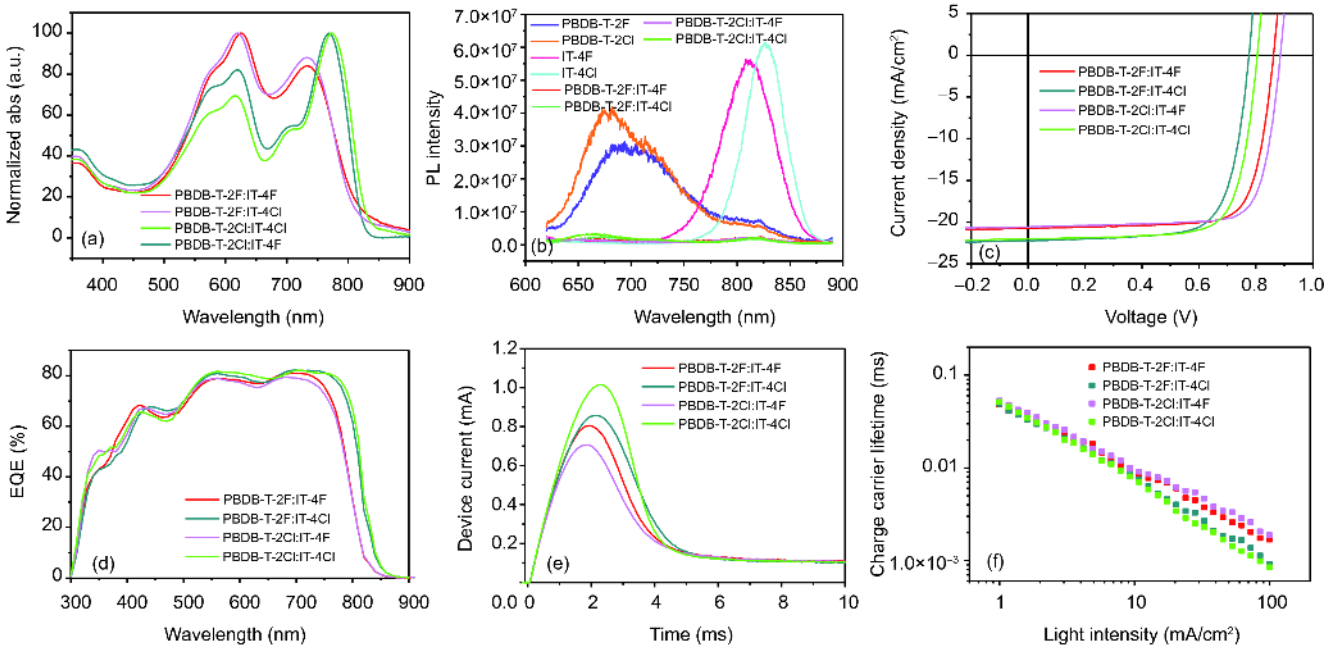

Figure 5 (a) Normalized absorption spectra of the four blend films. (b) Photoluminescence spectra of the neat films and their blend films. (c) *J*-*V* and (d) EQE curves of the four OSCs. (e) Photo-CELIV plot of four devices used to calculate carrier mobilities. (f) Plots of carrier lifetime as a function of light intensity for the four devices acquired from TPV measurements (color online).

Table 1 The photovoltaic parameters of four devices

Donor	Acceptor	V_{oc} (V)	J_{sc} (mA cm^{-2})	FF	PCE (%)	J_{sc} (mA cm^{-2})[a)]
PBDB-T-2F	IT-4F	0.86	20.80	0.76	13.59 (13.28±0.06)	19.92
	IT-4Cl	0.78	22.25	0.73	12.67 (12.39±0.02)	20.83
PBDB-T-2Cl	IT-4F	0.89	20.58	0.78	14.29 (13.96±0.04)	19.11
	IT-4Cl	0.81	22.01	0.74	13.37 (13.19±0.08)	21.07

a) Calculated J_{SC} from the EQE spectra shown in Figure 5(d).

J_{SC} for the four OSCs are resulted from the variances of the absorption range of the blends, which can be verified by the external quantum efficiency (EQE) measurements. As the V_{OC} is directly proportional to the difference between the HOMO level of the donor and the LUMO of the acceptor, the four OSCs show varied V_{OC} from 0.78 to 0.89 V according to the donor:acceptor energy level alignments. The difference between HOMO level of PBDB-T-2Cl and LUMO level of IT-4F leads to the highest V_{OC} while the combination of PBDB-T-2F:IT-4Cl-based device shows the lowest V_{OC}. PBDB-T-2Cl:IT-4F yields the highest V_{OC} of 0.89 V, and the PBDB-T-2F:IT-4Cl obtains the lowest V_{OC} of 0.78 V. All the FF of four OSCs are up to 0.70 with the highest value of 0.78 achieved for PBDB-T-2Cl:IT-4F-based device. The FFs of IT-4Cl-based OSCs are slightly lower than that of IT-4F-based devices. As a result, a representative PCE of 14.29% is recorded for PBDB-T-2Cl:IT-4F-based OSCs. The PBDB-T-2F:IT-4F-, PBDB-T-2Cl:IT-4Cl- and PBDB-T-2F:IT-4Cl-based OSCs yield representative PCEs of 13.59%, 13.37% and 12.67%, respectively. As depicted in Figure 5(d), IT-4Cl-based OSCs show broader response range with higher EQE values in the long wavelength region than IT-4F-based OSCs. The integrated current densities for the IT-4F- and IT-4Cl-based OSCs have good consistency with the *J*-*V* measurements, as provided in Table 1. We also analyzed efficiency distribution over 50 devices. And the statistics data (Figure S3) present efficiencies of OSCs based different donor:acceptor combination are according with a Gaussian distribution.

3.4.2 *Charge transfer and carrier lifetime*

To further study the underlying origin of the difference in the

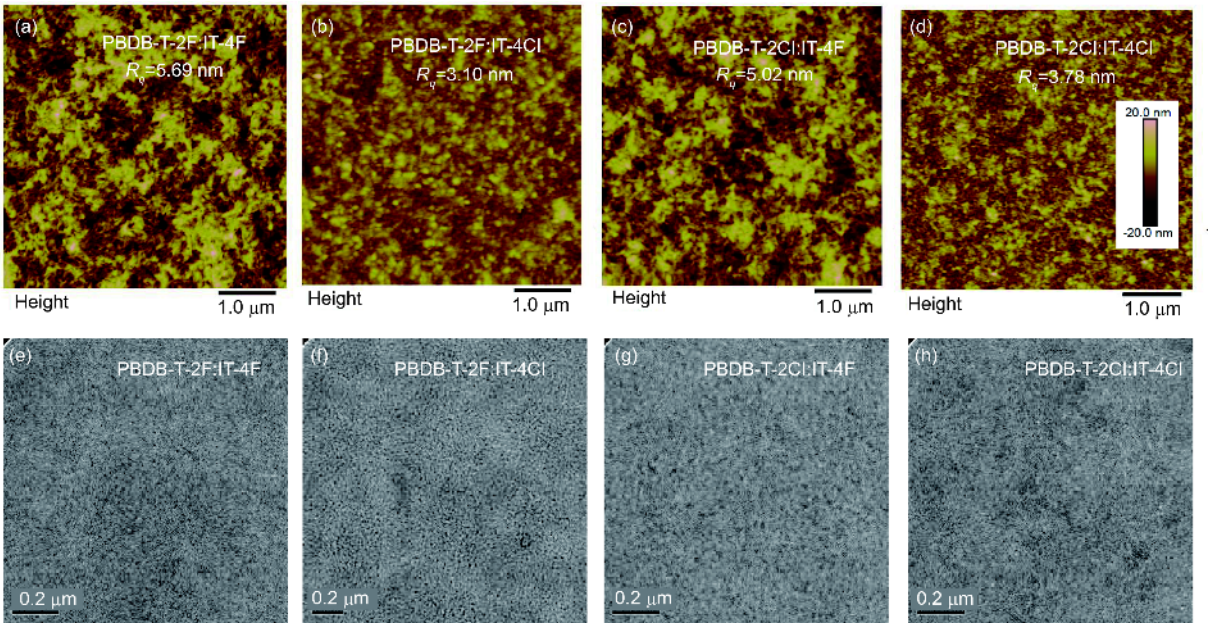

Figure 6 Morphology characterization of the blend films. (a–d) AFM height images and (e–h) TEM patterns for the four donor:acceptor blends (color online).

FF of the OSCs, we conducted the photo-induced charge extraction linearly increasing voltage (photo-CELIV) [66] and transient photovoltage (TPV) measurements. From the Figure 5(e), we can find that the IT-4F based two OSCs show much higher charge-carrier densities than IT-4Cl based OSCs. The carrier mobilities of PBDB-T-2Cl:IT-4F-, PBDB-T-2F:IT-4F-, PBDB-T-2Cl:IT-4Cl- and PBDB-T-2F:IT-4Cl-based devices are estimated to be 5.6×10^{-4}, 4.4×10^{-4}, 3.6×10^{-4}, and 1.9×10^{-4} cm^2 V^{-1} s^{-1}, suggesting that the mobilities of fast carrier component in the IT-4F-based blends are higher than that of IT-4Cl-based blends. As depicted in Figure 5(f), the charge carrier lifetimes of the four blends are measured as a function of light intensities. As the four OSCs show few differences on charge carrier lifetimes at varied light intensities, we were fitting these data linearly. The two IT-4Cl-based devices display higher slopes (−0.85 for PBDB-T-2F:IT-4Cl-based device and −0.91 for PBDB-T-2Cl:IT-4Cl-based device) than IT-4F-based devices (−0.74 for PBDB-T-2F:IT-4Cl-based device and −0.72 for PBDB-T-2Cl:IT-4Cl-based device), implying that more seriously recombination exist in the IT-4Cl-based devices. Under 100 mW cm^{-2} illumination (one sun), the PBDB-T-2Cl:IT-4F-, PBDB-T-2F:IT-4F-, PBDB-T-2Cl:IT-4Cl- and PBDB-T-2F:IT-4Cl-based devices show carrier lifetime of 1.88, 1.69, 0.84 and 0.92 μs. The higher charge carrier mobilities and longer lifetime in the IT-4F-based devices than that in the IT-4Cl-based devices may contribute to the higher FF.

3.4.3 Morphology characteristics

The surface and bulk morphology of the four donor:acceptor blend films were investigated by AFM and transmission electron microscopy (TEM). As shown in Figure 6(a–d), the AFM height images reveal that the four blend films have varied root-mean-square roughnesses (R_q) ranging from 3.10 to 5.67 nm. PBDB-T-2F:IT-4F- and PBDB-T-2Cl:IT-4F-based films show higher R_q than that of the other two blend films. From the TEM images, we can find that the four blend films show similar bicontinuous interpenetrating networks, which is benefit for the charge generation and transport in the devices.

4 Conclusions

In summary, we systematically study the difference between fluorination and chlorination on the properties of organic donors (PBDB-T-2F and PBDB-T-2Cl) and acceptors (IT-4F and IT-4Cl). In comparison with fluorination, chlorination has stronger ability in downshifting the molecular energy levels and boarding the absorption spectra. The impact of fluorination and chlorination on the crystalline properties is dependent on the introduction positions of halogen atoms. All of the donor:acceptor combinations show very good PCEs~13%–14% with litter difference. As chlorination is easier than fluorination in the view of synthesis, the material costs can be decreased, which benefits to the large-scale production for practical applications. Therefore, we think we should not ignore the chlorination when designing highly efficient photovoltaic materials, especially when its fluorinated counterpart has proved very good performance.

Acknowledgements This work was supported by the National Natural Science Foundation of China (91333204, 91633301, 51673201), the Ministry of Science and Technology of China (2014CB643501) and the Chinese Academy of Sciences (XDB12030200, KJZD-EW-J01).

Conflict of interest The authors declare that they have no conflict of interest.

Supporting information The supporting information is available online at http://chem.scichina.com and http://link.springer.com/journal/11426. The supporting materials are published as submitted, without typesetting or editing. The responsibility for scientific accuracy and content remains entirely with the authors.

1 Halls JJM, Walsh CA, Greenham NC, Marseglia EA, Friend RH, Moratti SC, Holmes AB. *Nature*, 1995, 376: 498–500
2 Yu G, Gao J, Hummelen JC, Wudl F, Heeger AJ. *Science*, 1995, 270: 1789–1791
3 Li G, Zhu R, Yang Y. *Nat Photon*, 2012, 6: 153–161
4 Heeger AJ. *Adv Mater*, 2014, 26: 10–28
5 Scharber M , Mühlbacher D, Koppe M, Denk P, Waldauf C, Heeger A , Brabec C . *Adv Mater*, 2006, 18: 789–794
6 Chen J, Cao Y. *Acc Chem Res*, 2009, 42: 1709–1718
7 Cheng YJ, Yang SH, Hsu CS. *Chem Rev*, 2009, 109: 5868–5923
8 Henson ZB, Müllen K, Bazan GC. *Nat Chem*, 2012, 4: 699–704
9 Li Y. *Acc Chem Res*, 2012, 45: 723–733
10 Fu Y, Wang F, Zhang Y, Fang X, Lai W, Huang W. *Acta Chim Sin*, 2014, 72: 158
11 Dou C, Liu J, Wang L. *Sci China Chem*, 2017, 60: 450–459
12 Lin Y, Zhan X. *Mater Horiz*, 2014, 1: 470–488
13 Fan H, Zhu X. *Sci China Chem*, 2015, 58: 922–936
14 Nielsen CB, Holliday S, Chen HY, Cryer SJ, McCulloch I. *Acc Chem Res*, 2015, 48: 2803–2812
15 Kang H, Lee W, Oh J, Kim T, Lee C, Kim BJ. *Acc Chem Res*, 2016, 49: 2424–2434
16 Li S, Zhang Z, Shi M, Li CZ, Chen H. *Phys Chem Chem Phys*, 2017, 19: 3440–3458
17 Zhang G, Zhao J, Chow PCY, Jiang K, Zhang J, Zhu Z, Zhang J, Huang F, Yan H. *Chem Rev*, 2018, 118: 3447–3507
18 Yao H, Ye L, Zhang H, Li S, Zhang S, Hou J. *Chem Rev*, 2016, 116: 7397–7457
19 Jiang W, Li Y, Wang Z. *Acc Chem Res*, 2014, 47: 3135–3147
20 Li G, Shrotriya V, Huang J, Yao Y, Moriarty T, Emery K, Yang Y. *Nat Mater*, 2005, 4: 864–868
21 Kim Y, Cook S, Tuladhar SM, Choulis SA, Nelson J, Durrant JR, Bradley DDC, Giles M, McCulloch I, Ha CS, Ree M. *Nat Mater*, 2006, 5: 197–203
22 Woo CH, Thompson BC, Kim BJ, Toney MF, Frechet JMJ. *J Am Chem Soc*, 2008, 130: 16324–16329
23 Duan C, Huang F, Cao Y. *J Mater Chem*, 2012, 22: 10416–10434
24 Wu JS, Cheng SW, Cheng YJ, Hsu CS. *Chem Soc Rev*, 2015, 44: 1113–1154
25 Lin Y, Wang J, Zhang ZG, Bai H, Li Y, Zhu D, Zhan X. *Adv Mater*, 2015, 27: 1170–1174
26 Cheng P, Li G, Zhan X, Yang Y. *Nat Photon*, 2018, 12: 131–142
27 Hou J, Inganäs O, Friend RH, Gao F. *Nat Mater*, 2018, 17: 119–128
28 Yan C, Barlow S, Wang Z, Yan H, Jen AKY, Marder SR, Zhan X. *Nat Rev Mater*, 2018, 3: 18003
29 Zhao W, Li S, Yao H, Zhang S, Zhang Y, Yang B, Hou J. *J Am Chem Soc*, 2017, 139: 7148–7151
30 Fan Q, Su W, Wang Y, Guo B, Jiang Y, Guo X, Liu F, Russell TP, Zhang M, Li Y. *Sci China Chem*, 2018, 61: 531–537
31 Xu X, Yu T, Bi Z, Ma W, Li Y, Peng Q. *Adv Mater*, 2018, 30: 1703973
32 Fei Z, Eisner FD, Jiao X, Azzouzi M, Röhr JA, Han Y, Shahid M, Chesman ASR, Easton CD, McNeill CR, Anthopoulos TD, Nelson J, Heeney M. *Adv Mater*, 2018, 30: 1705209
33 Li W, Ye L, Li S, Yao H, Ade H, Hou J. *Adv Mater*, 2018, 30: 1707170
34 Beaujuge PM, Fréchet JMJ. *J Am Chem Soc*, 2011, 133: 20009–20029
35 Chen HY, Hou J, Zhang S, Liang Y, Yang G, Yang Y, Yu L, Wu Y, Li G. *Nat Photon*, 2009, 3: 649–653
36 Wang Z, Zhu X, Zhang J, Lu K, Fang J, Zhang Y, Wang Z, Zhu L, Ma W, Shuai Z, Wei Z. *J Am Chem Soc*, 2018, 140: 1549–1556
37 Huo L, Zhou Y, Li Y. *Macromol Rapid Commun*, 2009, 30: 925–931
38 Yao H, Chen Y, Qin Y, Yu R, Cui Y, Yang B, Li S, Zhang K, Hou J. *Adv Mater*, 2016, 28: 8283–8287
39 Wang Y, Zhang Y, Qiu N, Feng H, Gao H, Kan B, Ma Y, Li C, Wan X, Chen Y. *Adv Energy Mater*, 2018, 26: 1702870
40 Yang F, Li C, Lai W, Zhang A, Huang H, Li W. *Mater Chem Front*, 2017, 1: 1389–1395
41 Zheng YQ, Wang Z, Dou JH, Zhang SD, Luo XY, Yao ZF, Wang JY, Pei J. *Macromolecules*, 2015, 48: 5570–5577
42 Li Y, Lin JD, Che X, Qu Y, Liu F, Liao LS, Forrest SR. *J Am Chem Soc*, 2017, 139: 17114–17119
43 Tang ML, Bao Z. *Chem Mater*, 2011, 23: 446–455
44 Tang ML, Oh JH, Reichardt AD, Bao Z. *J Am Chem Soc*, 2009, 131: 3733–3740
45 Zhang Q, Kelly MA, Bauer N, You W. *Acc Chem Res*, 2017, 50: 2401–2409
46 Reichenbächer K, Süss HI, Hulliger J. *Chem Soc Rev*, 2005, 34: 22–30
47 Liao SH, Jhuo HJ, Cheng YS, Chen SA. *Adv Mater*, 2013, 25: 4766–4771
48 Zhang S, Ye L, Zhao W, Yang B, Wang Q, Hou J. *Sci China Chem*, 2015, 58: 248–256
49 Chen Z, Cai P, Chen J, Liu X, Zhang L, Lan L, Peng J, Ma Y, Cao Y. *Adv Mater*, 2014, 26: 2586–2591
50 Liu Y, Zhao J, Li Z, Mu C, Ma W, Hu H, Jiang K, Lin H, Ade H, Yan H. *Nat Commun*, 2014, 5: 5293
51 Price SC, Stuart AC, Yang L, Zhou H, You W. *J Am Chem Soc*, 2011, 133: 4625–4631
52 Deng D, Zhang Y, Zhang J, Wang Z, Zhu L, Fang J, Xia B, Wang Z, Lu K, Ma W, Wei Z. *Nat Commun*, 2016, 7: 13740
53 Dai S, Zhao F, Zhang Q, Lau TK, Li T, Liu K, Ling Q, Wang C, Lu X, You W, Zhan X. *J Am Chem Soc*, 2017, 139: 1336–1343
54 Yao H, Cui Y, Yu R, Gao B, Zhang H, Hou J. *Angew Chem Int Ed*, 2017, 56: 3045–3049
55 Jia B, Dai S, Ke Z, Yan C, Ma W, Zhan X. *Chem Mater*, 2017, 30: 239–245
56 Xu SJ, Zhou Z, Liu W, Zhang Z, Liu F, Yan H, Zhu X. *Adv Mater*, 2017, 29: 1704510
57 Cui Y, Yang C, Yao H, Zhu J, Wang Y, Jia G, Gao F, Hou J. *Adv Mater*, 2017, 29: 1703080
58 Zhang H, Yao H, Zhu J, Li WW, Yu R, Gao B, Zhang S, Hou J. *Adv Mater*, 2018, http://doi.org/10.1002/adma.201800613
59 Mo D, Wang H, Chen H, Qu S, Chao P, Yang Z, Tian L, Su YA, Gao Y, Yang B, Chen W, He F. *Chem Mater*, 2017, 29: 2819–2830
60 Zhang S, Qin Y, Zhu J, Hou J. *Adv Mater*, 2018, 30: 1800868
61 Kawashima K, Fukuhara T, Suda Y, Suzuki Y, Koganezawa T, Yoshida H, Ohkita H, Osaka I, Takimiya K. *J Am Chem Soc*, 2016, 138: 10265–10275
62 Liu S, Kan Z, Thomas S, Cruciani F, Brédas JL, Beaujuge PM. *Angew Chem*, 2016, 128: 13190–13194
63 Blaskovits JT, Bura T, Beaupré S, Lopez SA, Roy C, de Goes Soares J, Oh A, Quinn J, Li Y, Aspuru-Guzik A, Leclerc M. *Macromolecules*, 2017, 50: 162–174
64 Sakamoto Y, Komatsu S, Suzuki T. *J Am Chem Soc*, 2001, 123: 4643–4644
65 Frisch MJ, Trucks GW, Schlegel HB, Scuseria GE, Robb MA, Cheeseman JR, Scalmani G, Barone V, Mennucci B, Petersson GA, Nakatsuji H, Caricato M, Li X, Hratchian HP, Izmaylov AF, Bloino J, Zheng G, Sonnenberg JL, Hada M, Ehara M, Toyota K, Fukuda R,

Hasegawa J, Ishida M, Nakajima T, Honda Y, Kitao O, Nakai H, Vreven T, Montgomery Jr JA, Peralta JE, Ogliaro F, Bearpark MJ, Heyd J, Brothers EN, Kudin KN, Staroverov VN, Kobayashi R, Normand J, Raghavachari K, Rendell AP, Burant JC, Iyengar SS, Tomasi J, Cossi M, Rega N, Millam NJ, Klene M, Knox JE, Cross JB, Bakken V, Adamo C, Jaramillo J, Gomperts R, Stratmann RE, Yazyev O, Austin AJ, Cammi R, Pomelli C, Ochterski JW, Martin RL, Morokuma K, Zakrzewski VG, Voth GA, Salvador P, Dannenberg JJ, Dapprich S, Daniels AD, Farkas Ö, Foresman JB, Ortiz JV, Cioslowski J, Fox DJ. Gaussian 09. Wallingford: Gaussian, Inc., 2009

66 Holliday S, Ashraf RS, Wadsworth A, Baran D, Yousaf SA, Nielsen CB, Tan CH, Dimitrov SD, Shang Z, Gasparini N, Alamoudi M, Laquai F, Brabec CJ, Salleo A, Durrant JR, McCulloch I. *Nat Commun*, 2016, 7: 11585